City Research Online

City, University of London Institutional Repository

Design of a compact polarization splitter by using identical coupled silicon nanowires

S. Soudi, *Member, IEEE*, and B. M. A. Rahman, *Fellow IEEE*

Abstract **Design of an ultra-compact polarization splitter (PS) based on silicon-on-insulator (SOI) platform is presented. The design incorporates two simply coupled identical silicon nanowires, which can be easily fabricated by using standard Complementary Metal-Oxide-Semiconductor (CMOS) technology and fully compatible with standard active silicon photonics platforms. It is shown here that a low-loss, 17.90 μm long compact PS, and wide bandwidth over the entire C-band can be achieved. Important waveguide design parameters such as the guide width, height and separation between them have been optimized, and modal birefringence and wavelength dependence have been calculated by using a full-vectorial H-Field finite element method. The optical power transfer characteristics have been calculated by using a rigorous least squares boundary residual method**.

Index Terms—**numerical analysis, finite element methods, nanophotonics, directional couplers, optical waveguides, silicon on insulator technology, polarization splitter.**

I. INTRODUCTION

OPTICAL systems incorporating rotationally symmetric optical fibers cannot maintain its polarization states as it encounters random bends, pressures, or manufacturing imperfections which allow power transfer between two orthogonally polarized modes. For many communication and sensing systems this creates a major problem where a specific polarization state is needed. In this case, a polarization independent or polarization diversity system would be useful.

Rather than pursuing difficult polarization-independent devices on SOI, alternatively a polarization diversity scheme could be employed [1]. TE/TM polarization splitters are important components for design and development of such polarization diversity optical systems, such as integrated-optic gyroscopes, switches, modulators and polarization independent receivers for coherent detection [2]. In this case, the orthogonal polarization components of the input light can first be split into two different waveguides by using a polarization splitter (PS). Following that, a polarization rotator (PR) [3] can be incorporated in one of the waveguides to rotate the polarization by 90°. Finally, for the rest of the optical system only one polarization needs to be processed. Therefore, on-chip optical polarization rotator and splitting are key functions for realizing polarization-transparent operation in photonic integrated circuits (PIC).

S. Soudi and B. M. A. Rahman are with the Department of Electrical and Electronic Engineering, City University, London EC 1V 0HB, U.K. (e-mail : sasan.soudi.1@city.ac.uk, and B. M. A. Rahman@city.ac.uk

II. DESIGN OF POLARIZATION SPLITTERS

For the design of polarization splitter the polarization dependent modal properties are exploited. An optical waveguide with small index contrast the resulting modal birefringence is smaller. However, this modal birefringence increases for high index contrast waveguide such as silicon nanowires. On the other hand, use of anisotropic materials, such as Lithium Niobate [4], or ion-exchanged glass [5] or use of metal cladding [6] can enhance the modal birefringence. Several metals such as gold, silver, copper, and aluminum, have been used to generate large birefringence, which can effectively shorten the dimension of optical components. However, metal-clad waveguides are also inherently lossy. It has also been shown that instead of using metal cladding by using simple layered isotropic material, material birefringence can also be introduced [7]. This modal birefringence can be exploited in the design of guided-wave polarization splitter, by incorporating y-splitter, directional coupler, Mach-Zehnder interferometer (MZI) or multimode interference (MMI) based designs. The designs of asymmetrical y-splitter in highly anisotropic lithium niobate were reported by Masuda and Yip [4] and Wei and Wang [8]. However, as the angle for a y-splitter needs to be smaller than 1 degree to avoid excessive power loss, often the resulting devices are relatively long.

Among the viable designs, a popular approach is to exploit the polarization dependent coupling of directional coupler because of their simplicity and easy design and also reasonable performance. Modal birefringence of optical waveguides produces polarization dependent coupling length which can be exploited to design polarization splitter. Small material birefringence of GaAs was exploited to design a 3000 μm long PS [9]. Metal clad can introduce strong modal birefringence and Albrecht *et al.* reported a 1600 μm long metal clad InP rib waveguide based asymmetrical directional coupler [10] and later on Rajarajan *et al.* reported a more compact 230 μm PS [11]. On the other hand, silicon waveguide can directly provide stronger shape birefringence Kiyat *et al.* reported an even more compact 120 μm PS using silicon rib waveguide [12].

Polarization splitters have also been designed by exploiting polarization dependent imaging distance of multimode MMI couplers. In an earlier work, simple modal birefringence was considered for an InP based design where the PS length was 1640 μm [13] and later on a shorter 1023 μm design was reported [14]. For a very narrow width MMI, supporting only two modes, which is also known as zero-gap directional

couplers or two modes coupler, a short PS can be designed [15].

MZI structures have also been considered for realizing PSs. In order to make a compact MZI a large birefringence is required. One of the earliest work, Soldano *et al*. reported [6] a 3300 μm MZ based PS using metal clad in one arm. Liang *et al*. [16] reported a 6000 μm long Mach-Zehnder design using natural modal birefringence of silicon rib waveguide and more recently Augustin *et al*. [17] reported a more compact 600 μm long design using higher waveguide birefringence of silicon nanowires incorporating MMI sections in MZI.

Recently there have been extensive research activities to develop silicon based photonics, by exploiting well developed CMOS technology. This can allow incorporation of both photonic and electronic components on the same chip. The high index contrast of silicon waveguides also allows more compact waveguides, bends and also other functional devices. But its modal characteristics are also strongly polarization dependent due to the strong index contrast. The dependence of the TE and TM polarizations can be exploited to find the polarization splitting ratio in order to design a compact PS.

Apart from strip silicon nanowires [18], silicon-based slot waveguides [19], where a low refractive index slot region placed between two silicon nanowires with high refractive index have been intensively investigated due to their unique opportunities and many potential applications. It can be noted that slot waveguides are also strongly polarization-dependent.

Recently, PSs based on horizontal single [20] and multi-slotted waveguide structures [21] have also been proposed. On the other hand, using an asymmetrical DC with a silicon wire and a vertical slot, a PS of 13.6 μm in length was demonstrated experimentally [22]. Dai [23] and Fukuda *et al*. [24] have considered asymmetric directional coupler with a NW and slot waveguide, ignoring very long coupling length for TE mode compared to TM modes. Besides these, polarization splitters incorporating hybrid plasmonic waveguides [25], waveguide bend [26], arrayed waveguide grating (AWG) [27], liquid crystal [28], photonic crystal [29] and grating couplers [30] have also been reported.

The Si polarization splitter proposed here shows a very compact design. It does not use slot guide, which is more difficult to fabricate, nor uses metal clad, which introduces loss, but uses two simple straight nanowires. In this paper, design optimization of a Si polarization splitter based on mature SOI technology is presented which requires less complex fabrication process with single mask only and backed by a well-established semiconductor industry [31]. Another benefit could arise in this design, due to the use of identical coupled waveguides, which are generally expected to be less sensitive to the fabrication tolerances.

III. THEORY

Pure TM or TE mode can only exist in planar slab waveguides (WGs) with one-dimensional confinement. However, in all practical optical WGs with two-dimensional confinement, the modes can be classified as quasi-TM and quasi-TE modes, which contain all six components of the **E** and **H** fields. Besides that, in high index contrast silicon nanowires, the modal birefringence is much higher. To calculate all the 3 components of the vector fields and the evolution of fully hybrid quasi-TE and quasi-TM modes along a guided-wave device all the methods to be employed should be fully vectorial in nature. Accurate calculations of the modal solution for the fundamental quasi-TE and quasi-TM modes are of significant importance when designing a PS. In the design of a compact PS, a full vectorial method is needed to obtain modal solutions of the supermodes and vectorial modal field profiles of the constituent NW waveguides across the dielectric interface. Since, all the three components of the **H**-field components are continuous across the dielectric interfaces such a full-vectorial formulation used here, based on the minimization of the **H**-field based energy functional [32]:

$$\check{S}^2 = \frac{\int \left[(\nabla \times \mathbf{H})^* \cdot v^{-1} (\nabla \times \mathbf{H}) + p(\nabla \cdot \mathbf{H})^* (\nabla \cdot \mathbf{H}) \right] dxdy}{\int \mathbf{H}^* \cdot \tilde{\ } \mathbf{H} \, dxdy} \qquad (1)$$

Where, **H** is the full-vectorial magnetic field, ^{2} is the eigenvalue where is the angular frequency of the wave, * denotes a complex conjugate and transpose, and and μ are the permittivity and permeability, respectively. The penalty term has also been included to reduce the appearance of spurious modes. In this paper, an in-house code incorporating these attractive features of this method is used to optimize the PS design. Although the FEM can be useful to calculate the propagation constants for the even and odd fundamental quasi-TE and quasi-TM supermodes and also their modal field profiles, however, alone, this method cannot analyze discontinuity along a guided-wave device. Although a full-vectorial beam propagation method (BPM) [33] can be used to calculate the power conversion between the two polarized modes, however, as the proposed structure being consists of only two discrete interfaces, a junction analysis method would be more efficient to use to find the excited modal coefficients at the junctions and to optimize the polarization splitter design. In this case, a powerful full-vectorial numerical approach, the Least Squares Boundary Residual (LSBR) method [34] has been used, which rigorously satisfies the continuity of the tangential magnetic and electric fields at the junction interface in a least squares sense. The LSBR approach looks for a stationary solution to satisfy the continuity conditions by minimizing the error energy functional, J, as given by [34], to satisfy the continuity conditions:

$$J = \int_\Omega \left| \mathbf{E}_t^I - \mathbf{E}_t^{II} \right|^2 + r \cdot Z_0^2 \left| \mathbf{H}_t^I - \mathbf{H}_t^{II} \right|^2 d\Omega \qquad (2)$$

Where Z_0 is the free-space impedance and is the dimensionless weighting factor to balance the electric and magnetic field components of the error functional J. In this case, the integration is carried out at the junction interface, , between the straight NW and the coupled Si waveguides. The LSBR method obtains the modal coefficients of the transmitted and reflected modes at the junction. This approach would be rigorous yet computationally more efficient than the use of the BPM.

V. PRINCIPLE

The PS proposed in this work is a very compact design

without a metal clad section or a bent or a slot and composed of two NWs of equal height identified by H. This would be easy to fabricate by using the mature CMOS technology, incorporating two simple coupled identical nanowires.

For a directional coupler, its coupling length, $L_c = \pi / (\beta_e - \beta_o)$, is the shortest length necessary for maximum energy transfer, where β_e and β_o are the propagation constants of the even and odd supermodes of the coupled structure. For most of the practical waveguides the coupling length for the quasi-TE and quasi-TM modes are different but for low-index contrast waveguides the difference is small. As stated earlier, for a high index contrast this difference could be relatively larger and additionally by using anisotropic material, or metal clad the difference can be increased further. For highly birefringent NWs the coupling length for quasi-TE or TM polarizations, L_c^{TE} and L_c^{TM} are significantly different and if we can have $L = m * L_c^{TE} = n * L_c^{TM}$, where m and n are integer and one of them is odd and other one even, then two orthogonally polarized waves will emerge from two different output ports, as shown in Fig.1. This condition may not be very difficult to achieve, but often yields larger m and n values. Performance error due to any fabrication tolerance is magnified by m or n, which often makes such design very sensitive to small changes in waveguide parameters. Here, our design target was to have m and n as small as possible, and for the best possible design to achieve $m = 1$ and $n = 2$. Hence, we seek a design where, the coupling length for quasi-TE (L_c^{TE}) polarization is twice that for the quasi-TM (L_c^{TM}) polarization, if possible, allowing most of the quasi-TE and quasi-TM polarized powers to emerge from bar port and cross-port, respectively.
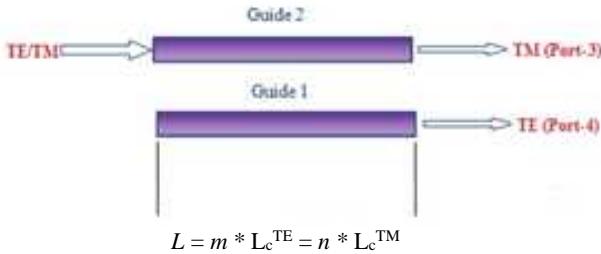

Fig . 1. Principle of a polarization splitter.

VI. RESULTS

The schematic cross-section of the coupled NWs is shown in Fig.2. Here, the width and height of the NW are shown by W and H, respectively and separation between the cores is shown as S. The refractive index of the Si and Silica are taken as 3.4754752 and 1.4440236, respectively, at the operating wavelength of 1.55 μm.

Here the existing symmetry condition of the coupled structure has been exploited for the modal solutions of the directional coupler. This not only avoids mode degeneration by separating two interacting modes, but also would obtain more accurate solutions, with a given computer resources. Since this structure has one-fold symmetry, only half of the waveguide needs to be considered, which will allow a much finer mesh division to be used. The combinations of **n×H** and **n.H** at the vertical symmetry line have been used to find the

even and odd supermodes. From the modal solutions the coupling lengths for the quasi-TE and quasi-TM polarizations, L_c^{TE} and L_c^{TM}, can be calculated and subsequently ratio of these coupling lengths, R_{TE-TM} (L_c^{TE} / L_c^{TM}) is also calculated. Like all other photonic devices, its performance will depend on the accuracy of the designs and also on the accuracy of the fabrication. However, design accuracy will also critically depend on the accuracy of the modal solutions. A small change of the separation distance (or its width and height) will not only change the quasi-TE and quasi-TM coupling lengths but also the R_{TE-TM}, which will affect the performance and these are discussed in this paper.

The optical propagation in a directional coupler can be expressed in terms of the propagation constants of the even and odd supermodes of the coupled structures, or their effective indices ($n_{eff} = \beta/k_0$, where k_0 is the wavenumber given by $2\pi/\lambda$), where n_{eff} (even) and n_{eff} (odd), and the effective indices of the even and odd supermodes, respectively. Accuracy of the L_c depends on the accuracy of the modal solutions, and more particularly on their differences, and it is critical that the accuracy of these parameters is established first. As most of the key design parameters are often obtained by using a given numerical method and it is also known that accuracy of these design parameters are also depend on the numerical parameters used, and as example, for the FEM the number of elements (or mesh divisions used) is the critical numerical parameter, and this is studied first.
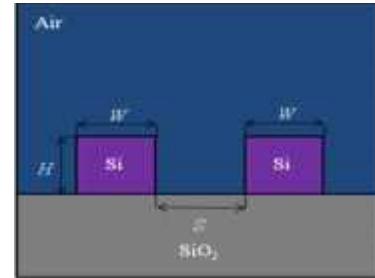

Fig . 2. Cross-section of two identical coupled NWs.

Variations of the effective indices, n_{eff} of the fundamental quasi-TE (H^y_{11}) even and odd supermodes for a silicon nanowire with the mesh division are shown in Fig. 3. In this case, the waveguide Height (H), Width (W) and Separation (S), are taken as 220 nm, 400 nm, and 100 nm, respectively. For simplicity equal number of mesh division is used in both the transverse directions. Variations of the $n_{e\text{-}TE}$ (even) and $n_{e\text{-}TE}$ (odd) are shown by a blue solid line and a red dash-dotted line, respectively. It can be observed that when the number of mesh increases, effective indices of both the fundamental quasi-TE supermodes increase. It can be noticed that, the effective index of TE even supermode is higher than that of the TE odd supermode (two different scales are used) and both reach their saturation points asymptotically. It should be noted that when a 200 * 200 mesh is used n_{eff} is accurate up to 3rd decimal place, and the accuracy is increased to 4th decimal place when mesh size is increased to 800 * 800.

Variations of the effective indices of the quasi-TM (H^x_{11}) even and odd supermodes are shown in Fig.4. In this case, the waveguide Height (H), Width (W) and Separation (S), are

taken as 220 nm, 400 nm, and 100 nm, respectively. Variations of the n_{e-TM} (even) and n_{e-TM} (odd) are shown by a blue solid line and a red dash-dotted line, respectively. It can be observed here that as the mesh refinement is increased initially the effective index values increased, however, with a finer mesh rapidly converge to their saturation values. It should be noted that the range of effective index variation for the quasi-TM modes are relatively smaller than that of the quasi-TE modes shown in Fig.3.
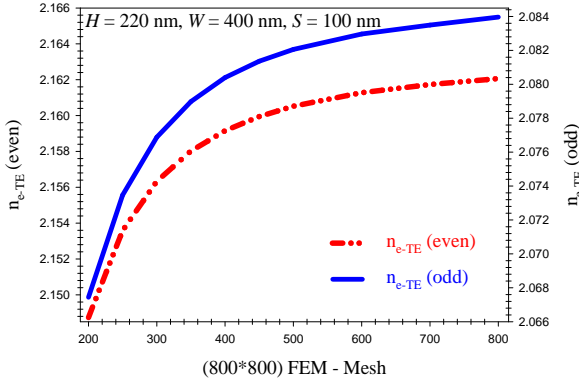

Fig. 3. Variations of the effective indices of the quasi-TE even and odd supermodes with the mesh.
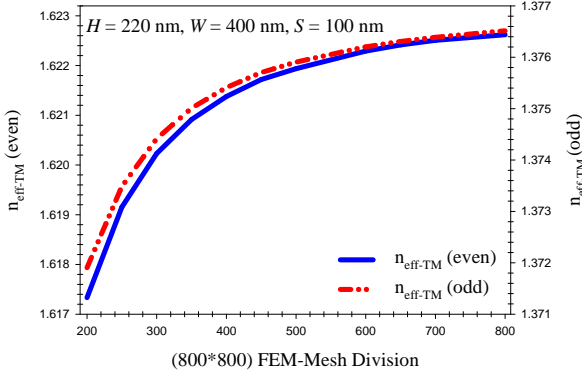

Fig. 4. Variations of the effective indices of the quasi-TM even and odd supermodes with the mesh.
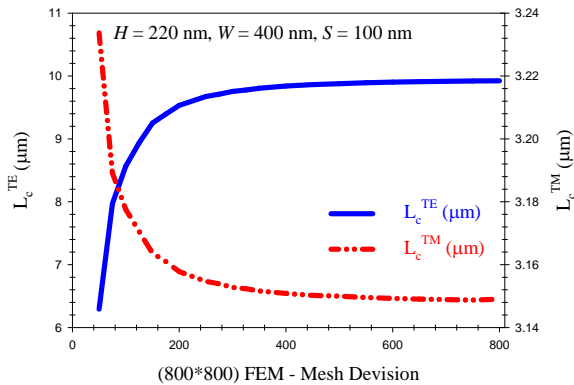

Fig. 5. Variations of the coupling lengths for the quasi-TE and quasi-TM polarizations with the mesh.

From these modal solutions, coupling lengths of both quasi-TE and quasi-TM polarizations, L_c^{TE} and L_c^{TM}, respectively, can be calculated. Variations of the coupling lengths for the fundamental quasi-TE and quasi-TM polarizations for $H = 220$ nm, $W = 400$ nm and $S = 100$ nm with the mesh

division are shown in Fig. 5. A blue solid and a red dash-dotted line represent L_c of the quasi-TE and quasi-TM-polarizations, respectively. It can be observed from Fig. 5, that as the number of mesh is increased from 100 to 500, initially the L_c^{TE} (solid) increases rapidly, but, with further increase in the number of mesh, the L_c^{TE} reaches a stable values asymptotically, but for the L_c^{TM} curve (dash-dotted) decreases exponentially as a number of mesh increases from 100 to 800, and reaches its stable value about 3.149 μm. Two separate scales are used for L_c^{TE} and L_c^{TM}, and it should be noted that changes in their values are rather small. It can also be observed that L_c^{TM} variation is more stable with the mesh, and this is due to the fact that the fundamental quasi-TM (H^x_{11}) mode being close to its cut-off its variations with the waveguide's geometrical and numerical parameters is small.

Next, for the design of a polarization splitter the L_c ratio (R_{TE-TM}) is calculated from the polarized coupling lengths, L_c^{TE} / L_c^{TM}. Variation of this coupling length ratio (R_{TE-TM}) for $H = 220$ nm, $W = 400$ nm and $S = 100$ nm with the mesh division is shown in Fig. 6. It can be noticed that as the number of the mesh division is increased, initially this ratio increases appreciably and then converges to its stable value. It can be noted that L_c ratio (R_{TE-TM}) is accurate up to the second decimal point when 800 * 800 mesh divisions are used. Following this all the numerical simulations are carried out using equivalent to or better than 800 * 800 mesh divisions in the two transverse directions, where more than 1.2 million first-order triangular elements have been employed to represent the half of the waveguide structures. In these cases, the horizontal and vertical mesh resolutions are better than 1 nm and 0.5 nm, respectively. We have bench-marked our mode solver code with the polarization splitter design reported by Fukuda *et al.* [24]. We have obtained the L_c^{TE} and L_c^{TM} values as 135.0 μm and 11.0 μm for the quasi-TE and quasi-TM modes, respectively and Fukuda *et al.* reported their device length between 10 ~ 15 μm.

Variations of the R_{TE-TM}, with the waveguide width for three different heights, 260 nm, 280 nm and 300 nm, are shown in Fig. 7 by a solid blue line, a red dashed line and a black dash-dotted line, respectively with the same separation- $S = 150$ nm. It can be noticed that as the waveguide width increases, the $R_{TE-TM,}$ also increases. It can be noted that it is possible to obtain an ideal $R_{TE-TM} = 2.00$, when quasi-TE and quasi-TM modes can emerge from two different ports. However, care must be taken to make sure that the numerically simulated results are accurate. For $H = 260$ nm, 280 nm and 300 nm, when $R_{TE-TM} = 2.00$ is achieved then the corresponding waveguides widths would be 315 nm, 311 nm and 314 nm, respectively and for these three cases the device lengths would be equal to 4.940 μm, 5.235 μm and 6.180 μm, respectively. It can be noted that for $H = 260$ nm, there is a small discontinuity in the R_{TE-TM} curve, which was identified as the point where H^x_{11} and H^y_{21} modes are degenerate.

On the other hand, variations of the R_{TE-TM} with the waveguide height are shown in Fig. 8 by a blue solid line for $W = 315$ nm, a dash-dotted red line for $W = 314$ nm and a dashed black line for $W = 311$ nm (but for the same $S = 150$ nm), respectively. From these figures, a design relationship can also be achieved such that the coupling length for the quasi-TE polarization is exactly twice that of the quasi-TM

polarization. The non-monotonic changes of the L_c ratio has been identified to the modes approaching their cut-off conditions when the Height, *H*, was considerably lower. To understand the non-monotonic nature of R_{TE-TM} variation as shown in Fig. 8, next, their individual coupling lengths are also presented. Variations of the coupling lengths as a function of the waveguide heights for the quasi-TE and quasi-TM polarizations are shown in Fig. 9 by a solid blue line and a red dashed dotted line, respectively. The quasi-TE and quasi-TM coupling lengths are shown by using two different scales. The coupling length for quasi-TE polarization presented by using the left-hand Y–axis shows a usual near linear variation of the coupling length. This is because, reduction in height increases evanescent field outside waveguide core, resulting stronger mode coupling and as a result, coupling length reduces. Variation of the quasi-TM coupling length is shown in Fig. 9 by using its right-hand Y-axis. Here, it can be observed that as the waveguide height is reduced, initially L_c reduces slowly with the height and then reaches a minimum value of 2.43 µm at H = 260 nm, then increases slightly as mode approaches its cut-off point (quasi-TM mode approaches cut-off earlier). This non-monotonic variation of L_c^{TM} causes a similar non-monotonic variation of their L_c ratio, R_{TE-TM}, as shown earlier in Fig. 8. It can be observed from this figure that for a given width (say W = 315 nm) there can be two different waveguide heights which satisfy the design requirement of ratio, R_{TE-TM} to be exactly 2.00. However, their performances, such as device lengths and more importantly the effects of fabrication tolerances could be different.

Variations of the coupling lengths ratio, R_{TE-TM}, with the waveguide separation for the quasi-TE and quasi-TM polarizations are shown in Fig. 10. The black short dashed, blue solid and long dashed red lines represent the H = 260 nm, 280 nm and 300 nm, with corresponding waveguide widths are 315 nm, 311 nm, and 314 nm, respectively. It can be observed from this figure that, as the separation between the waveguides is increased from 50 nm to 150 nm, the coupling lengths ratio, R_{TE-TM} increases. At higher separations, as the guides are nearly isolated, the modal birefringence does not change any more with the waveguide separation. From Fig. 10, again a design relationship can be achieved such that R_{TE-TM} = 2.00. It can be noticed from this figure that for the waveguide heights, H = 260 nm, 280 nm and 300 nm, the separation between the guides, *S*, should be 150 nm to get the ideal value, R_{TE-TM} = 2.00. In these cases, the polarization splitter length should be equal to 4.940 µm, 5.235 µm and 6.180 µm, respectively.

Although the short device length can yield a compact polarizer, but it is also necessary to study their fabrication tolerances in order to understand their suitability for practical applications. Like all other photonic devices, its performance depends on the accuracy of fabrication. A small change in the width (or its height or their separation) would not only change their quasi-TE and quasi-TM polarization coupling lengths but also change the L_c ratio (R_{TE-TM}) from its desired value of 2.00. Performances of such PS against the fabrication tolerances related to its height, width and separation can be evaluated. A possible design was identified, when H = 280 nm, W = 311 nm, and S = 150 nm, resulting, L_c^{TE} = 5.235 µm and L_c^{TM} = 2.605 µm, giving R_{TE-TM} =2.00. So, following an accurate fabrication if the device length is equal to 5.235 µm, then, it is expected that quasi-TE mode will emerge from the Cross-port (Port 4) and quasi-TM mode in the Bar-port (Port 3).

At first, the variations of the quasi-TE power outputs in the Cross-port (P_{4-TE}) and Bar-port (P_{3-TE}) and quasi-TM outputs in the Cross-port (P_{4-TM}) and Bar-port (P_{3-TM}) as a function of separation between the waveguides are calculated, initially, by using a simple semi-analytical approach by considering their changes in the coupling lengths only. Later a more rigorous full-vectorial approach is used to find these values more accurately.
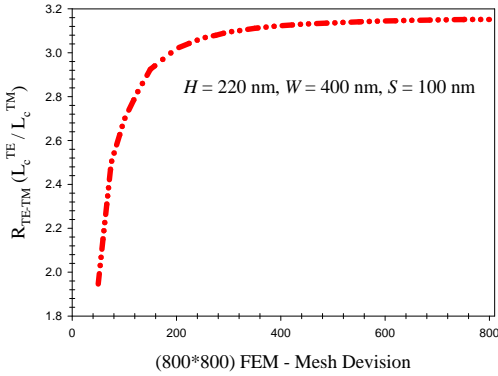

Fig. 6. Variation of the coupling length ratio of the quasi-TE and quasi-TM supermodes with the mesh.
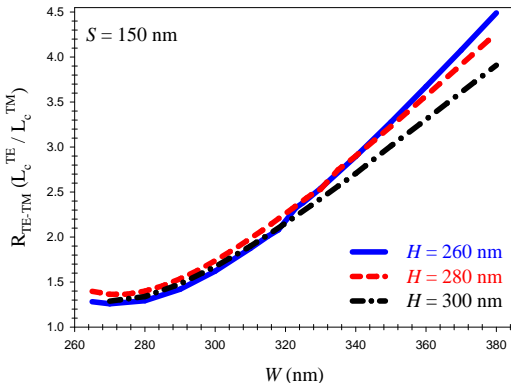

Fig. 7. Variations of the coupling length ratios of the quasi-TE and quasi-TM supermodes with the waveguide width for different heights.
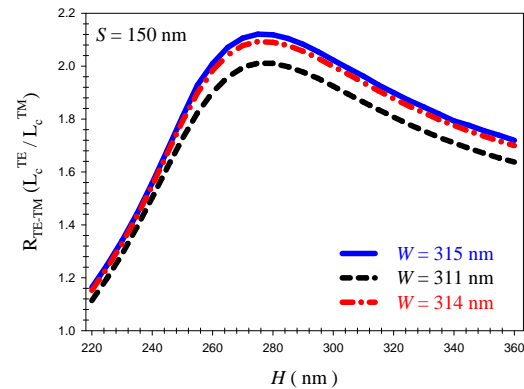

Fig. 8. Variations of the coupling length Ratio, R_{TE-TM}, with the waveguide height for the different widths.
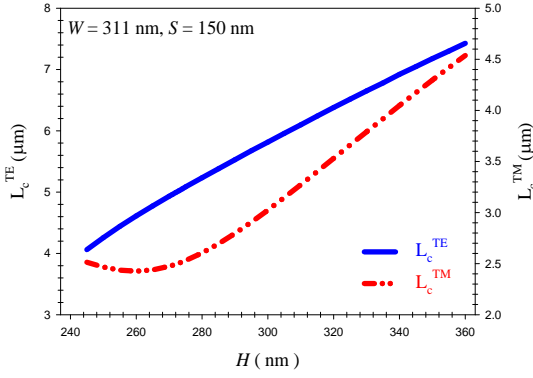
Fig. 9. Variations of the coupling lengths with the waveguides heights.

Figure 11 shows the variations of the power transfer as a function of the separation between the waveguides, when $H = 280$ nm and $W = 311$ nm, and the device length is kept fixed at $L = 5.235$ µm, as designed. As can be observed from this figure, when, $S = 150$ nm, as planned, at device length is equal to $L = L_c^{TE}$ $2 * L_c^{TM} = 5.235$ µm, for both quasi-TM polarization for quasi-TE polarization, most of the power will emerge from the Bar-port ($P_{3\text{-}TM}$) and in the Cross-port ($P_{4\text{-}TE}$), shown by red dashed-dotted and blue solid lines, respectively. Also, the black dashed-dotted and the green dashed lines show the quasi-TE power transfer characteristics in Port 3 ($P_{3\text{-}TE}$) and the quasi-TM power transfer characteristics in port 4 ($P_{4\text{-}TM}$), respectively. As can be seen from the figure, at the end of the coupling length, for both quasi-TM and quasi-TE polarized modes, almost zero power remained in Bar-port ($P_{4\text{-}TM}$) and Cross-port ($P_{3\text{-}TE}$). Therefore, by careful selection of the device parameters, a desired design for the polarization splitter is obtained. It can be noticed from these curves that a small change in waveguide separation can deteriorate the device performances. This phenomenon can be explained with the help of Fig. 10. It can be noticed that as the waveguides separation is deviated from the design value of the $R_{TE\text{-}TM}$ value of 2.00, not only the ratio will increases, but also the resulting coupling length would not match with the device length and hence deteriorate of the power transfer characteristics. This also shows power output for the quasi-TM mode is more sensitive compare to the quasi-TE polarization power mode, as here n being twice of m, the phase error for quasi-TM mode mismatch would be double that of the quasi-TE mode.
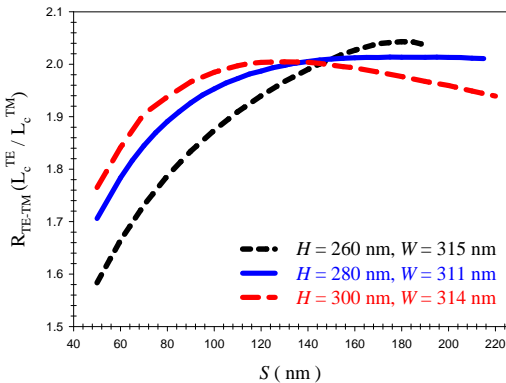

Fig. 10. Variations of the coupling length Ratio, $R_{TE\text{-}TM}$, with the waveguide separation, S.

However, the power output not only depends on the coupling length or the coupling length ratio, but also on the modal coefficients of the supermodes excited at the start of the directional coupler. To satisfy the continuity of the tangential electric and magnetic fields, E_t and H_t, an incident mode not only generates two supermodes but may also excite other higher-order guided or radiating modes. In this study a rigorous full-vectorial least squares boundary residual method [34] is used to find the modal coefficients of the two supermodes. From the modal coefficients, their propagation constants and full vectorial modal field profiles the evolution of quasi-TE and quasi-TM power along the waveguide branches can be calculated more rigorously. Variations of the TE and TM power in Port 4 and Port 3, with the propagation distance are shown in Fig.12. It can be observed that at $Z = 0$, 96% of the input TE power is coupled to Port 3 as shown by a solid blue line and this value reduces along the propagation distance. At a distance $Z = L = L_c^{TE}$, most of this power has been transferred to Port 4, shown by a red dashed-dotted line. Similarly, at $Z = 0$, nearly 81% of the input TM power was coupled to Port 3, as shown by a green dashed-dotted line, however, at a distance $Z = L = 2 * L_c^{TM}$, most of this returns to Port 3, since this distance is double of its coupling length. On the other hand, TM power in port 4, shown but a black dashed line, shows its maximum value at $Z = L / 2 = L_c^{TM}$.

Any deviation from the ideal design will not only change the coupling lengths, and their ratio, but also the modal coefficients of the excited modes in the directional coupler section. From the modal coefficients, their propagation constants and full vectorial modal field profiles the evolution of quasi-TE and quasi-TM power along the waveguide branches can be calculated more rigorously. Figure 13 shows the variation of the power transfer for different separations between the waveguides for $H = 280$ nm and $W = 311$ nm. The red dashed-dotted line $P_{4\text{-}TE}$ (LSBR) and the dark green dashed-dotted-dotted line $P_{3\text{-}TM}$ (LSBR) show the power transfer characteristics for the quasi-TE and polarized modes in the Cross-port (Port 4) and quasi-TM mode in the Bar-port (Port 3), respectively. From the rigorous LSBR method, the transmitted coefficients C_y^e and C_y^o for the quasi-TE even and odd supermodes are obtained as 0.83536 and 0.67721, respectively, when $S = 150$ nm. In this case, for the quasi-TE mode power transfer to Cross-Port ($P_{4\text{-}TE}$) was 92 %, represent only 0.40 dB loss. The transmitted coefficients of the even and odd quasi-TM supermodes are obtained as 0.81770 and 0.58613, respectively, and 77 % power transferred to Bar-Port ($P_{3\text{-}TM}$) with a loss value of 1.10 dB. For references, the results by using simple analytical approach, only considering the changes in the coupling length are shown again in Fig. 13 by solid blue and black dashed lines. In this case, it can be noticed that transfer of quasi-TM mode in Port 3 has deteriorated significantly compared to the power transfer of quasi-TE mode in Port 4. It should be noted that for such typical nanowires, as often height is smaller than its width, the effective index of the fundamental quasi-TM (H_{11}^x) mode is much lower than that of the fundamental quasi-TE (H_{11}^y) mode. This had contributed to a smaller coupling length for quasi-TM polarization, but this has also resulted in stronger coupling between the guides. It is well known that for a strong coupled directional coupler cross-talk increases due to

incomplete cancellation of modal fields in the two waveguides, and similarly in this case power loss for the quasi-TM polarization has been higher.
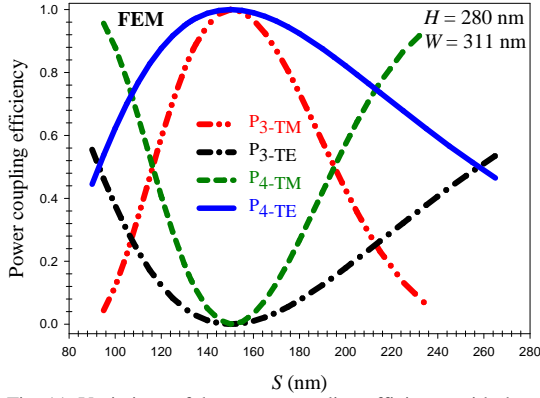

Fig. 11. Variations of the power coupling efficiency with the separation.
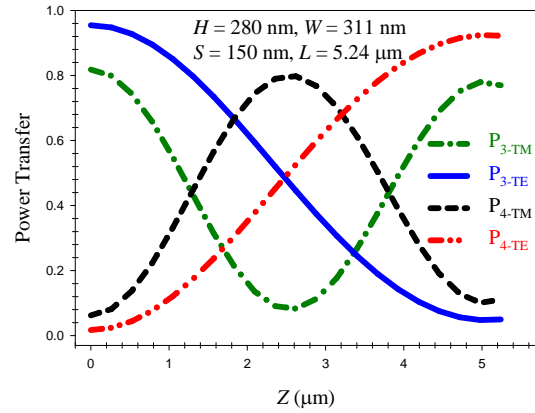

Fig. 12. Variations of the quasi-TE and quasi-TM powers in Ports 4 and 3 along the axial direction.
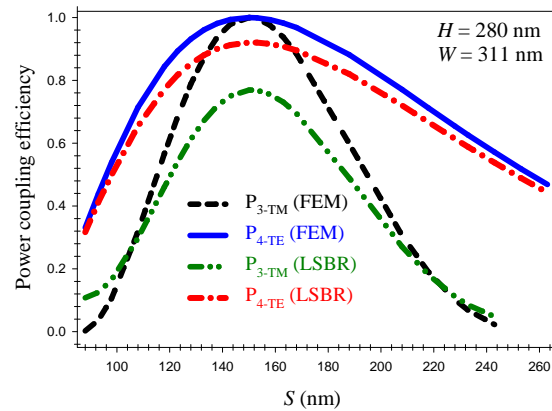

Fig. 13. Variations of the power coupling efficiency with the changes in the separation, S.

Therefore, it is expected that by reducing the coupling for both quasi-TE and quasi-TM polarized modes, it may be possible to reduce the power loss for both the polarizations. However, coupling lengths for both the quasi-TE and quasi-TM modes will increase which will make the device length a bit longer. Besides that L_c ratio will also change, however, it is still possible to achieve the desired L_c ratio (R_{TE-TM}) of 2.00 by adjusting other waveguide parameters, such as, its width and height. Figure 14 shows the variation of the power transfer

for the quasi-TE and quasi-TM polarized modes as a function of the waveguide separation by using the LSBR method. In this case, its height was kept fixed at 300 nm, and width was adjusted to achieve R_{TE-TM} = 2.00 for a given separation. It can be noticed that, by increasing the separation between the waveguides width, transferred power of quasi-TE polarized mode to the Port - 4 and quasi-TM polarized mode into the Port - 3 are increased. It can be noticed from this figure that when the separation between the guides change from the 140 nm to the 300 nm, the power transfer increased from the 0.9415 to 0.9543 for the quasi-TE input in Port-4 and from 0.8055 to 0.8429 for the quasi-TM polarized modes in Port-3, respectively. At the same time, the cross-talk improved from -18.6 dB to -26 dB for the quasi-TE input and from -13 dB to the -20 dB for the quasi-TM polarized modes, respectively (but not shown here). The black dashed-dotted curve in Fig. 14 shows the coupling length for the quasi-TE mode (the right-hand Y –axis scale) as a function of the waveguide separation. It can be seen from this figure that, as the separation between the guides is increased from 140 to 300 nm, the coupling length ($L = L_c^y$) increases linearly from 5.0 µm to 17.9 µm.

Weak coupling can also make the device sensitive with the fabrication tolerances. Therefore, it may be necessary to control the separation of these waveguides within a few nanometers, and sensitivity of this parameters, must be studied. Variation of the power transfer for the different separation between the waveguides for H = 300 nm, W = 317 nm and L = 17.9 µm are studied next, and shown in Fig. 15. The solid blue shows the quasi-TE power transfer characteristics in Port 4 (P_{4-TE}) by using the LSBR result. The dashed red line shows that the quasi-TM power transfer characteristics in Port 3 (P_{3-TM}). In this case most of the quasi-TE polarized power transferred to Cross-Port (P_{4-TE}) with only 0.21 dB loss and quasi-TM power into Bar-Port (P_{3-TM}) with 0.74 dB loss. It can be noticed that from this curve that the deterioration of the quasi-TM power transfer characteristics (P_{3-TM}) is more severe than the quasi-TE case. It can be noted that quasi-TE output power in Cross-Port is better than 50 % of its maximum value, when separation is in the range of 240 nm to 400 nm. On the other hand quasi-TM output in the Bar-Port is better than 50 % of its maximum value, when separation is between 275 nm to 340 nm. This narrower quasi-TM range is due to n being double of m. In Fig. 15, the green dashed-dotted line shows the cross-talk in the Bar-port (P_{3-TE}) for the quasi-TE case and the dashed-dotted black line shows the cross-talk in the Cross-port (P_{4-TM}), for the quasi-TM polarization mode, calculated by the LSBR method. It can be noticed that change in separation can deteriorate the cross-talk for the both cases, but this also shows cross-talk for quasi-TM mode is more sensitive compare to the quasi-TE mode. As can be seen from this figure, when S = 300 nm, at the end of the device length, for both the quasi-TE and quasi-TM modes, almost zero power remained in Port 3 and Port 4, respectively. Effects of width and height variations were also studied but not shown here. It can be noted that when its height changed by ± 20 nm from the design value of 280 nm, the quasi-TE power transfer was better than 80% of its maximum value. Similarly when the change in the width is ± 20 nm from its design value of 311

nm, quasi-TE mode power transfer was also better than 80% of its maximum value. However, power transfer for the quasi-TM mode was more sensitive and its height and width changes need to be within ± 10 nm for the same 80% power transfer limit.

This structure has been optimized for the operating wavelength of λ = 1550 nm. Any changes in the operating wavelength will change the coupling length, coupling length ratio and also the supermode coefficients. Figure 16 illustrates the power transfer as a function of the operating wavelength. This figure shows the coupled power in the bar and cross ports for the quasi-TE and quasi-TM polarizations, respectively.
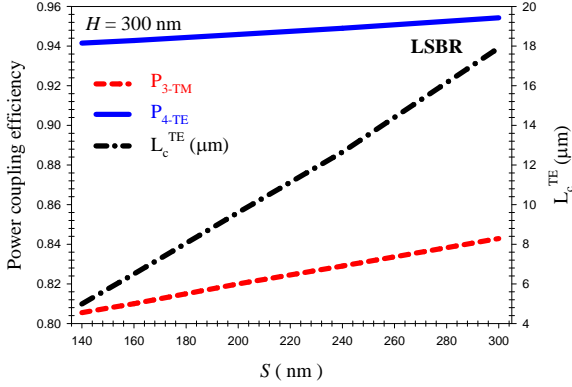

Fig.14. Variation of the power transfer for the quasi-TM and quasi-TE modes, and coupling length of the quasi-TE mode with the waveguide separations, S.
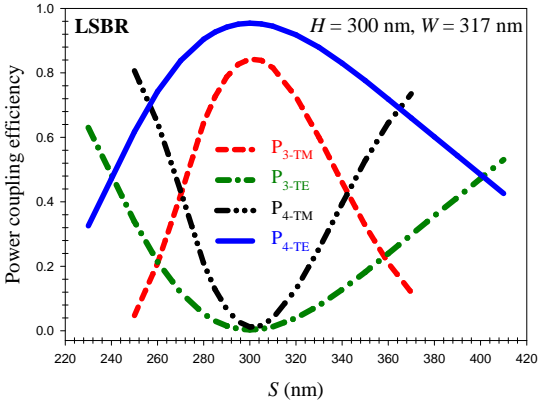

Fig.15. Variation of the power transfer for the different separations between the waveguides, for H = 300 nm and W = 317 nm.

Since there is a weaker coupling for quasi-TE polarization compare to quasi-TM polarization, the response for quasi-TE polarization is broadband. Figure 16 shows that, the crosstalk in the Cross-port smaller for quasi-TE mode than that in the Bar-port for quasi-TM mode, because the confinement of the quasi-TE mode is stronger than the quasi-TM mode. It can be noticed from these curves that as the wavelength changes, power transfer characteristics also changes and this will also change the phase matching conditions. However, it is shown here that, the effect of small change in the wavelength is quite small. This indicates that for many practical applications the device will have a larger operating bandwidth. The effect of temperature variation has also been studied for this device but this is not presented here. It was identified that a small amount of temperature tuning may be possible, which can be used to

compensate fabrication tolerances, but the tuning range is rather very limited. Similarly, as Fig.16 indicates a small amount of wavelength tuning can also be used to compensate the fabrication tolerances.

VII. CONCLUSION

The design presented in this work uses two identical silicon nanowires, which would be simpler than the design approaches reported earlier by using slot waveguides [20-23]. As the proposed structure does not consider any bent section or slanted side wall [18], and [31], or trench with different etch depth [12, 17, 31] so, it would be easier to fabricate. No metal clad has been used which avoids plasmonic modal loss.
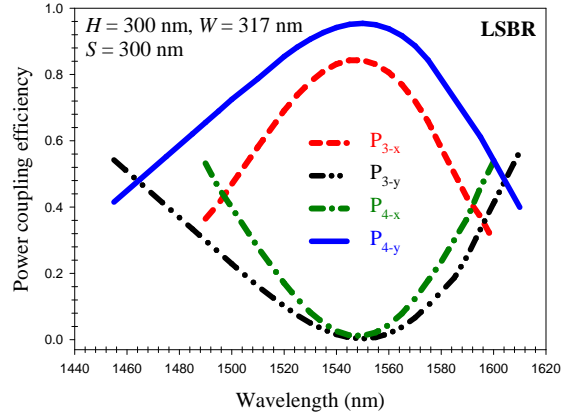

Fig. 16.Variation of the power transfer with the wavelength for H = 300 nm, S = 150 nm and W = 317 nm.

Two identical waveguides are used which shows better fabrication tolerances. This design approach is optimized by using rigorous numerical approaches. The above results suggest that an appreciable short 17.90 μm long PS can be designed at the 1.55 μm wavelength by adjusting the coupling lengths ratio of the quasi-TE and quasi-TM polarized modes. Device parameters are optimized in such a way that the PS length is equal to odd and even multiples of the coupling length for two different polarizations. Important fabrication parameters such as the height, width, separation, birefringence and wavelength sensitivity have been rigorously verified and their operating characteristics are shown. Maximum power transfer of 96 % for the quasi-TE polarized and 85 % for the quasi-TM polarized modes from input TE/TM mode, with crosstalk better than - 26 dB and loss value lower than 0.2 dB. It is shown here that, it is necessary for all the numerical methods; the stability of the numerical parameters should be established before the design process. Thus this high conversion efficiency, low footprint, simpler design, along with the use of well-matured fabrication technologies for SOI structures, should make the proposed design attractive for making an on-chip polarization splitter for their potential deployment. This design should be relatively easy to implement for fabrication and can be made with a single mask. It is also shown here that operating bandwidth of these PS is considerable wider and suitable for WDM application.

VIII. References

[1] T. Barwicz, M. R. Watts, M. A. Popovi , P. T. Rakich, L. Socci, F. X. Kärtner, E. P. Ippen, and H. I. Smith, "Polarization-transparent microphotonic devices in the strong confinement limit," *Nat. Photonics* **1** , pp. 57–60 , Dec. 2007.

[2] B. Glance, "Polarization independent coherent optical receivers," *J. Lightw. Technol.*, vol. 5, no. 2, pp. 274–276, Feb. 1987.

[3] S. Soudi, and B. M. A. Rahman, "Design of compact polarization rotator using simple silicon nanowires*,*" *Appl. Opt.* vol. 53, no. 34, pp. 8071-8077, Dec. 2014.

[4] M. Masuda, and G. L. Yip, "An optical TE-TM mode splitter using a LiNbO$_3$ branching waveguide*,*" *Appl. Phys. Lett.*, vol. 37, no.1, pp. 20-22, Jul. 1980.

[5] A. N. Miliou, R. Srivastava, and R. V. Ramaswamy, "A 1.3-µm directional coupler polarization splitter by ion exchange," *J. Lightw. Technol.*, vol. 11, no. 2, pp. 220–225, Feb. 1993.

[6] L. B. Soldano, A. H. de Vreede, M. K. Smit, B. H. Verbeek, E. G. Metaal, and F. H. Groen, "Mach-Zehnder Interferometer polarization splitter in InGaAsP/InP," *IEEE Photon. Technol. Lett.*, vol. 6, no. 3, pp. 402-405, Mar. 1994.

[7] M. Rajarajan, and B. M. A. Rahman, and K. T. V. Grattan, "A novel and compact optical polarizer incorporating a layered waveguide core structure," *J. Lightw. Technol.*, vol. 21, no. 12, pp. 3463–3470, Dec. 2003.

[8] P. Wei, and W. Wan., "A TE-TM mode splitter on lithium niobate using Ti, Ni, and MgO diffusions," *IEEE Photon. Technol. Lett.*, vol. 6, no. 2, pp. 245-248, Feb. 1994.

[9] F. Ghirardi, J. Brandon, M. Carre, A. Bruno, L. Menigaux, and A. Carenco, "Polarization splitter based on modal birefringence in InP/InGaAsP optical waveguides," *IEEE Photon. Technol. Lett.*, vol. 5, no. 9, pp. 1047-1049, Sep. 1993.

[10] P. Albrecht, M. Hamacher, H. Heidrich, D. Hoffman, H. P. Nolting, and C. M. Weinert., "TE/TM mode splitters on InGaAsP/InP," *IEEE Photon. Technol. Lett.*, vol. 2, no. 2, pp. 114-115, Feb. 1990.

[11] M. Rajarajan, C. Themistos, B. M. A. Rahman, and K. T. V. Gratan, "Characterization of metal-clad TE/TM mode splitters using the finite element method," *J. Lightw. Technol.*, vol. 15, no. 12, pp. 2264-2269, Dec. 1997.

[12] I. Kiyat, A. Aydinli, and N. Dagli, "A compact silicon-on-insulator polarization splitter," *IEEE Photon. Technol. Lett.*, vol. 17, no. 1, pp. 100–102, Jan. 2005.

[13] B. M. A. Rahman, N. Somasiri, C. Themistos, and K. T. V. Grattan, "Design of optical polarization splitter in a single-section deeply etched MMI waveguides," *Appl. Phys. Lett.* vol. 73, no. 5, pp. 613-618, Oct. 2001.

[14] J. M. Hong, H. H. Ryu, S. R. Park, J. W. Jeong, S. G. Lee, E. Lee, S. Park, D. Woo, S. Kim, and O. Beom-Hoan, "Design and fabrication of a significantly shortened multimode interference coupler for polarization splitter application," *IEEE Photon. Technol. Lett.*, vol. 15, no. 1, pp. 72-74, Jan. 2003.

[15] B. K. Yang, S. Y. Shin, and D. Zhang, "Ultrashort polarization splitter using two-mode interference in silicon photonic wires," *IEEE Photon. Technol. Lett.*, vol. 21, no. 7, pp. 432-434, Apr. 2009.

[16] T. K. Liang and H. K. Tsang., "Integrated polarization beam splitter in high index contrast silicon-on-insulator waveguides," *IEEE Photon. Technol. Lett.*, vol. 17, no. 2, pp. 393-395, Feb. 2005.

[17] L. M. Augustin, R. Hanfoug, J. J. G. M. van der Tol, W. J. M. de Laat, and M. K. Smit," A compact integrated polarization splitter/converter in InGaAsP-InP," *IEEE Photon. Technol. Lett.*, vol. 19, no. 17, pp. 1286-1288, Sep. 2007.

[18] D. Dai, Y. Shi, and S. He, "Characteristic analysis of nanosilicon rectangular waveguide for planar light-wave circuits of high integration," *Appl. Opt.* vol. 45, no. 20, pp. 4941-4946, Jul. 2006.

[19] V. R. Almeida, Q. Xu, C. A. Barrios, and M. Lipson, "Guiding and confining light in void nanostructure," *Opt. Lett.*, vol. 29, no. 11, pp. 1209-1211, Jun. 2004.

[20] Y. Fei, S. Chen, L. Zhang, and T. Cao, "Design and analysis of polarization splitter based on a horizontal slotted waveguide," *Opt. Eng.*, vol. 51, no. 5, pp. (054601-1)-(054601-4), May 2012.

[21] J. Xiao, X. Liu, and X. Sun, "Design of a compact polarization splitter in horizontal multiple-slotted structure," *J. Appl. Phys.*, vol. 47, no. 5, pp. 3748–3754, May 2008.

[22] S. Lin, J. Hu, and K. B. Crozier, "Ultracompact broadband slot waveguide polarization splitter," *Appl. Phys. Lett.*, vol. 98, no. 15, pp. (151101-1)-(151101-3), Apr. 2011.

[23] D. Dai, Z. Wang, and J. E. Bowers, "Ultrashort broadband polarization beam splitter based on an asymmetrical directional coupler," *Opt. Lett.*, vol. 36, no. 13, pp. 2590-2592, Jul. 2011.

[24] H. Fukuda, K. Yamada, T. Tsuchizawa, T. Watanabe, H. Shinojima, and S. Itabashi, "Ultrasmall polarization splitter based on silicon wire waveguides, *Opt. Express*, vol. 14, no. 25, pp. 12401-12408, Dec. 2006.

[25] X. Guan, H. Wu, Y. Shi, and D. Dai, "Extremely small polarization beam splitter based on a multimode interference coupler with a silicon hybrid plasmonic waveguide," Opt. Lett., 39, no. 2, pp.259-262, 2014.

[26] C. Van Dam, L. H. Spiekman, F. P. G. M. van Ham, F. H. Groen, J. J. G. M. van der Tol, I. Moerman, W. W. Pascher, M. Hamacher, H. Heidrich, C. M. Weinert, and M. K. Smit, "Novel compact polarization converters based on ultra short bends," *IEEE Photon. Technol. Lett.*, vol. 8, no. 10, pp. 1346-1348, Oct. 1996.

[27] W. N. Ye, D. X. Xu, S. Janz, P. Waldron, P. Cheben, and N. G. Tarr, "Passive broadband silicon-on-insulator polarization splitter," *Opt. Lett.*, vol. 32, no. 11, pp. 1492–1494, May 2007.

[28] Q. Wang, G. Farrell, and Y. Semenova, "Design of integrated polarization beam splitter with liquid crystal," *IEEE J. Sel. Topics Quantum Electron.*, vol. 12, no. 6, pp. 1349–1353, Nov. 2006.

[29] Y. Shi, D. Dai, and S. He, "Proposal for an ultracompact polarization-beam splitter based on a photonic-crystal-assisted multimode interference coupler," *IEEE Photon. Technol. Lett.*, vol. 19, no. 11, pp. 825-827, Jun. 2007.

[30] Y. Zhang, Y. He, J. Wu, X. Jiang, R. Liu, C. Qiu, X. Jiang, J. Yang, C. Tremblay, and Y. Su, "High-extinction-ratio silicon polarization beam splitter with tolerance to waveguide width and coupling length variations," Optics Express, 24, pp.6586-6593, Mar. 2016.

[31] D. Dai, L. Liu, S. Gao, D. Xu, and S. He, "Polarization management for silicon photonic integrated circuits," *Laser Photon. Rev.*, vol. 7, no. 3, pp. 303-328, may 2013.

[32] B. M. A. Rahman, and J. B. Davies, "Finite element solution of integrated optical waveguides," *J. Lightw. Technol.,* vol. LT-2, no. 5, pp. 682-688, Oct. 1984.

[33] S. S. A. Obayya, B. M. A. Rahman, and H. A. El-Mikati, "New full-vectorial numerically efficient propagation algorithm based on the finite element method," *J. Lightw. Technol.,* vol. 18, no. 3, pp. 409-415, Mar. 2000.

[34] B. M. A. Rahman and, J. B. Davies, "Analysis of optical waveguide discontinuities," *J. Lightw. Technol.* vol. 6, no.1, pp. 52-57, Jan. 1998.

IX. Biographies

B. M. Azizur Rahman received BSc Eng. and MSc Eng. degrees in Electrical Engineering with distinctions from Bangladesh University of Engineering and Technology (BUET), Dhaka, Bangladesh, in 1976 and 1979, respectively. He also received two gold medals for being the best undergraduate and graduate student of the University in 1976 and 1979, respectively. He received his PhD degree in Electronic Engineering from University College, London in 1982. From 1976 to 1979, he was a Lecturer at the Electrical Engineering Department, BUET. After completing his PhD he joined University College London as a Post-doctoral Research Fellow and continued his research work on the finite element modeling of optical waveguide until 1988. In 1988, he joined the Electrical, Electronic and Information Engineering Department of City University, London, as a Lecturer, where he is now a Professor. Prof. Rahman has published more than 500 journal and conference papers and his journal papers have been cited more than 3300 times. Prof. Rahman is a Fellow of the Institute of Electrical and Electronic Engineers (IEEE) in USA, Optical Society of America (OSA), and the Society of Photo-optical Instrumentation Engineers (SPIE).

S. Soudi received the BSc Eng. degree in Electronics, and MSc Eng. degree in Nuclear, from Islamic Azad University-Iran in 1994 and 2000, respectively. From 2001, he worked at Islamic Azad University in Iran – Abhar Branch as a faculty member. He received his PhD degree in Electronic - Nano Photonics Engineering from City University London in 2015. He is member of IEEE, OSA, and SPIE. His current research interests include Silicon micro-/nano-photonic integrated devices.